# scientific reports



# **OPEN**

# A highly efficient hybrid fiber optic laser using a cesium atom vapor cell as an optical gain medium

Seokjin Kim<sup>1</sup>, Mingyu Lee<sup>1</sup>, Sanggwon Song<sup>1</sup>, Seongjin Hong<sup>2</sup>, Johan Nilsson<sup>3⊠</sup> & Kyunghwan Oh<sup>1,4⊠</sup>

A new scheme of a highly efficient hybrid laser cavity is proposed and experimentally demonstrated utilizing a hot cesium (Cs) vapor cell as an optical gain medium. The laser cavity consists of a macroscopic concave reflector (>99% reflectivity) and a 4% Fresnel-reflecting facet of a single mode fiber (SMF). The cesium gain cell is located between these two reflectors. The SMF serves multiple roles: (1) a passive mode-matching component to approximate the pump beam diameter to that of the laser cavity mode within the cesium cell, (2) an output coupler with a low reflectivity, and (3) a low loss laser delivery with a high beam-quality. Optimizing the pump beam waist diameter and the cesium vapor cell temperature, a high slope efficiency of 86% and an optical-to-optical conversion efficiency of 71% were achieved in the pump power range of 400–600 mW. The unique multi-functional role of the SMF in the hybrid cavity is fully described, which can also be applied to other high optical gain media.

**Keywords** Alkali atom vapor, Atom laser, Laser efficiency, Fiber optics, Hybrid cavity

#### Abbreviations

SMF Single mode fiber
LDs Laser diodes
HC Hybrid cavity
MR Macroscopic reflector

ECDL External cavity diode laser
BS Beam splitter

DM Dichroic mirror AR Anti-reflection APC Angled physical contact PC Physical contact PM Power meter OC Output coupler ALAspheric lens **LMAF** Large-mode-area fiber

Atomic gas lasers featured prominently in early laser physics research<sup>1</sup>, but their efficiency was limited by poorly optimized pumping, such as electrical gas discharge, flash, and arc lamps. The recent development of laser diodes (LDs) and their stable high-power operation in array configurations<sup>2,3</sup> have provided an attractive pumping scheme for a wide range of lasers. LD-pumping has been implemented in various optical gain media, including rare-earth-doped fiber lasers<sup>4,5</sup>, solid-state lasers<sup>6,7</sup>, and gas lasers<sup>8</sup>. In particular, rare-earth-doped fiber lasers have been a primary beneficiary of LD-pumping, obtaining high power and efficiency. This unique combination of LD and fiber optics has led to rapid development of various high-power fiber lasers that are now used in many industrial, medical, military, and scientific applications<sup>9,10</sup>.

Meanwhile, fiber-coupled optical gain media have been studied in solid, liquid, and vapor phases to further advantage the optical fibers' superb light guidance capability  $^{11-17}$ . Optically coupling the gain medium of the macroscopic scale (~10mm in diameter) to an optical fiber (~10  $\mu$ m in the core diameter) has provided excellent

<sup>1</sup>Photonic Device Physics Laboratory, Department of Physics, Yonsei University, 50 Yonsei-ro, Seodaemun-Gu, Seoul 03722, Korea. <sup>2</sup>Department of Physics, Chung-Ang University, 47 Heukseok-ro, Dongjak-Gu, Seoul 06974, Korea. <sup>3</sup>Optoelectronics Research Centre, University of Southampton, Southampton SO17 1BJ, UK. <sup>4</sup>Department of Physics, School of Sciences and Humanities Nazarbayev University, 53, Kabanbay batyr Ave, 010000 Astana, Republic of Kazakhstan. <sup>△</sup>email: jn@orc.soton.ac.uk; koh@yonsei.ac.kr

light confinement and guidance control, improving laser efficiency  $^{12,14}$  and output power  $^{15,17}$ . Optical fibers are also used for low-loss delivery of the laser output, maintaining a well-defined laser spot size, brightness, and polarization over various distances  $^{18}$ . Incessant development of LDs, optical fibers, and innovative combinations are still revolutionizing laser technologies  $^{19-22}$ .

Researchers have been further exploring using LDs to pump the atomic vapor, which requires narrow spectral linewidth and wavelength stability<sup>23</sup>. If those requirements are met, alkali atom vapors can show their intrinsic potential to offer a high quantum efficiency<sup>24,25</sup>. Since the first demonstration of the alkali atom vapor laser<sup>26</sup>, various types of laser cavities and pumping schemes have been explored to demonstrate how atomic optical gain can be transformed into practical laser systems. Longitudinal pumping schemes, which use LD arrays in multiple paths and directions, have been studied as a way to increase the absorbed pumping power<sup>27–29</sup>. Stable and unstable cavities with transverse LD-pumping schemes have also been investigated for laser power scaling<sup>30–32</sup>. The cavity parameters have been investigated to enhance slope efficiency, such as optimizing the output coupler transmittance<sup>33</sup> and reducing cavity losses by utilizing Brewster angle windows for the vapor cell<sup>34</sup>. Additionally, improvements in slope efficiency have been reported through fine adjustments and frequency locking of the pump laser<sup>35</sup>. Despite the notable achievement of kilowatt-level output power, the slope efficiency of previous attempts based on LD-pumping has been significantly lower than the quantum limit of alkali atoms<sup>36–38</sup>. These results contrast the slope efficiency achieved with a bulky Ti:Sapphire laser pumping in early research<sup>39</sup>. Probable reasons for this discrepancy could be mainly attributed to the spatial mismatch between the laser cavity modes and the LD pump beam within the gain medium. This mismatch can limit the conversion of the pump photons, reducing the net optical gain and, subsequently, the laser slope efficiency<sup>25</sup>. Nonlinear ionization processes in high-power pumping<sup>24</sup> are known to result in additional loss, which limits the laser efficiency.

Recent advances in maximizing the optical gain of alkali atom vapor amplifiers have included the adaptation of SMFs $^{40-42}$ . This approach has successfully matched the spatial distribution of the signal and pump laser beams to maintain a high spatial overlap in the optical gain medium in a single-pass amplifier. The critical merit of using SMF was to guide both the pump and signal in the  $LP_{01}$  mode of SMF since their wavelengths are separated by only  $\sim 40$  nm to allow the fundamental mode guidance to both beams. This light guidance over SMF resulted in a substantial increase in the amplification factor  $^{41}$  and output power of the amplifier  $^{42}$ . However, fiber optic spatial beam control has yet to be attempted in lasers, where the laser modes defined by the cavity boundary conditions should be considered instead of signal lasers.

In this study, the authors have introduced a novel fiber optic approach to experimentally demonstrate a highly efficient cesium (Cs) atom vapor laser. We accomplished this by implementing a hybrid cavity (HC), a unique combination of a macroscopic reflector (MR), a microscopic SMF, and a macroscopic atom vapor cell placed between them for the first time. The unique SMF-MR-HC provided new rationales in laser technology: (1) An efficient passive spatial mode-matching: SMF-MR-HC secured the high spatial mode overlap over 90% between the pump and laser cavity mode inside the cesium vapor cell. The proposed scheme successfully approximated the pump beam diameter to that of the laser cavity mode with a stable accuracy within the vapor gain medium, which has not been attempted in previous atom vapor laser cavities. (2) An optimal output coupling: SMF provides a low reflectivity of ~ 4% Fresnel reflection at the cleaved end facet to satisfy the optimal output coupling ratio for a cesium vapor gain medium, which was not achieved in prior dielectric mirrors. (3) A high beam-quality laser output delivery: The SMF also transmits the laser output in the fundamental  $LP_{\theta 1}$  mode to ensure high beam quality, inherently solving the laser output beam-quality issues in prior technologies.

By optimizing the HC's physical parameters, the authors achieved a significant enhancement in the laser slope efficiency, overcoming one of the oldest hurdles in atom vapor lasers. The report covers the design principles of the HC, the laser's performance, and a comparison with previous laser cavities.

# **Experimental setup**

Figure 1 shows a schematic diagram of the experimental configuration. We used an external cavity diode laser (ECDL, Toptica DLC pro) as a pump laser. It had a spectral linewidth of 100 kHz and a tuning range of 12 GHz around  $\lambda_P$ =852 nm, corresponding to the D<sub>2</sub> transition,  $6^2\mathrm{S}_{1/2} \rightarrow 6^2\mathrm{P}_{3/2}$  of the cesium atom. See the bottom right inset of Fig. 1. We used an absorption spectroscopy feedback scheme<sup>35</sup>, where pump laser power (~1 µW) tapped from a beam splitter (BS) was monitored as it propagated through a cesium reference cell, "Cell 1". The pump laser frequency was locked to the minimum transmission at the total angular momentum F=4 transition. See the inset bottom left. The dichroic mirror (DM) transmitted the pump laser at 852 nm and reflected the laser at  $\lambda_L$ =894 nm, corresponding to the transition,  $6^2\mathrm{P}_{1/2} \rightarrow 6^2\mathrm{S}_{1/2}$ . An aspheric lens "AL 1" with a focal length of 13 mm focused the pump laser to SMF end facet. The SMF was Corning 780HP, whose  $LP_{11}$  mode cutoff wavelength was ~730±30 nm, ensuring the fundamental  $LP_{01}$  mode guidance for both  $\lambda_P$  =852 nm and  $\lambda_L$ =894 nm. One of SMF ends was terminated with an angle to form an anti-reflection (AR) coated angled physical contact (APC) connector, preventing unwanted optical feedback. The other end of the SMF was terminated with an uncoated perpendicular facet and mounted in a standard physical contact (PC) connector. The power of the laser beam was measured by a power meter, PM (Thorlabs, S145C).

Our proposed HC consisted of a concave spherical macroscopic reflector (MR) with a 100 mm radius of curvature (R $\sim$ 99.7%) and the perpendicularly cleaved facet of SMF, whose reflectivity is  $\sim$ 4%. It uniquely combines the stable high reflectivity of the MR and multi-functional fiber optic output coupler (OC). The SMF guided both the laser output at  $\lambda$  = 894 nm and the pump at  $\lambda$  = 852 nm in its fundamental  $LP_{01}$  mode.

The optical boundaries, the MR surface, and the fiber OC defined the laser modes of our proposed HC. The optical gain was provided by "Cell 2" between them. The frequency-locked pump laser propagated through the SMF in the fundamental  $LP_{01}$  mode and exited toward "Cell 2", which could be approximated as a Gaussian beam  $^{43,44}$ . The pump beam waist diameter was fine-tuned using the aspherical lens "AL 2" with a focal length of

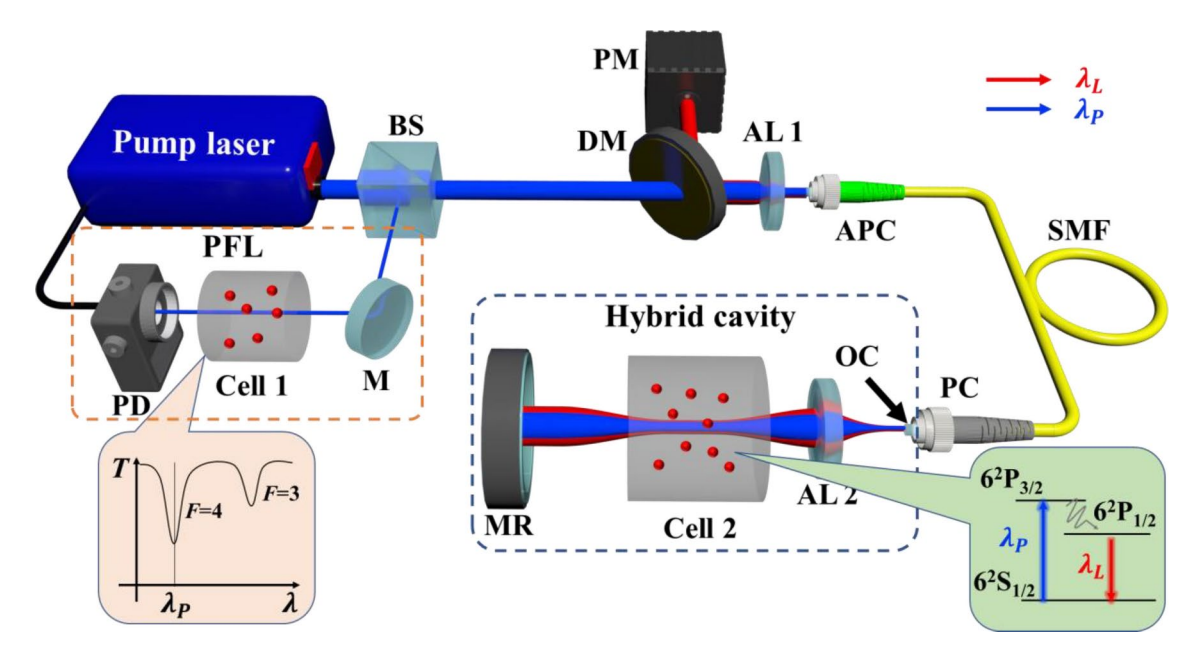


**Fig. 1.** The schematic diagram of the experimental setup for HC laser. The setup comprises a laser "cavity" and a "spectroscopy". The cavity consists of a macroscopic reflector (MR), and the end facet of single mode fiber (SMF) terminated at an uncoated physical contact (PC) connector. The spectroscopy unit locks the pump laser frequency to the atomic transition. (BS: beam splitter, M: mirror, PD: photodetector, PM: power meter, PFL: pump laser frequency locking, DM: dichroic mirror, SMF: single mode fiber, AL: aspheric lens APC: Angled physical contact connector, PC: Physical contact connector, OC: output coupler, MR: macroscopic reflector, *F*: total angular momentum).

2 mm and an adjustable position. Note that the surfaces of the aspheric lenses ("AL 1" and "AL 2") were all ARcoated to suppress optical feedback.

The optical gain medium, "Cell 2," was a glass cylinder with an axial length of 2 cm and a diameter of 2.5 cm. It was filled with cesium and 66 kPa of ethane buffer gas. The buffer gas collision broadened the cesium absorption spectrum<sup>45</sup> and accelerated the non-radiative decay from  $6^2P_{3/2}$  to  $6^2P_{1/2}^{44}$ . The cell windows were AR-coated at 852 nm and 894 nm. An electric heater enclosing the cell in the lateral direction controlled the vapor temperature from 100 to 140 °C.

The CW lasing started when the pump power increased over the threshold condition. The output was guided in the SMF's  $LP_{01}$  mode and passed through the AR-coated APC. The laser was reflected toward the PM at the DM.

Optimizing the pump beam waist within the optical gain medium was critical to enhance the laser efficiency since it determines the overall pump absorption and the gain dynamics in the 3-level optical gain system<sup>45</sup> as in the cesium vapor. The pumping rate is insufficient for a collimated pump beam with an excessively large waist. In contrast, when the pump beam is too tightly focused, the pump extends the beam waist rapidly after the focal point, diminishing the overall pumping rate before it reaches the other end of the cell. By changing the distance between the SMF facet and the "AL 2" with an adjustable fiber collimator (Thorlabs, CFC2-B), the pump beam waist diameter and its axial location were optimized within the optical gain medium, "Cell 2".

### Results and discussion

The laser characteristics were measured for various pump beam waists (defined by  $1/e^2$  intensity level), and the results are summarized in Fig. 2. Here, we set the "Cell 2" temperature at 120 °C. The temperature variation was suppressed under one °C using a commercial temperature controller. The incident pump power was measured after the "AL 2". See Fig. 1. The pump beam waist was located at the center of "Cell 2". A beam profiler (Thorlabs, BP104-IR) measured the pump beam waist diameter. The concave mirror location and, subsequently, the cavity length were also optimized for maximum output power. Experimental cavity parameters of the proposed hybrid laser are summarized in Table 1. In the experiments, we kept the reflectance ( $R \sim 99.7\%$ ) and the radius of curvature (100 mm) of MR the same. The laser output power reached its maximum of 419 mW at the pump beam waist of 90 µm with 7.5 mm Rayleigh length, and the corresponding pump threshold was 103 mW. Note that the available pump power limited the laser output power.

Optimally focused pump beam diameter could provide the highest pumping rate, which is inversely proportional to the local pump beam area  $^{46}$ . See Fig. 2a. The slope efficiency was plotted as a function of the pump beam waist in Fig. 2b. We obtained a maximum slope efficiency of  $86.5 \pm 0.04$  at the pump beam waist of 90  $\mu$ m. As the pump beam waist diameter further increased to  $120~\mu$ m, the laser power reduced to 302~mW and the slope efficiency to 60.1%. We attributed this behavior to the variation of the pump beam area and its volume overlapping the cesium atoms.

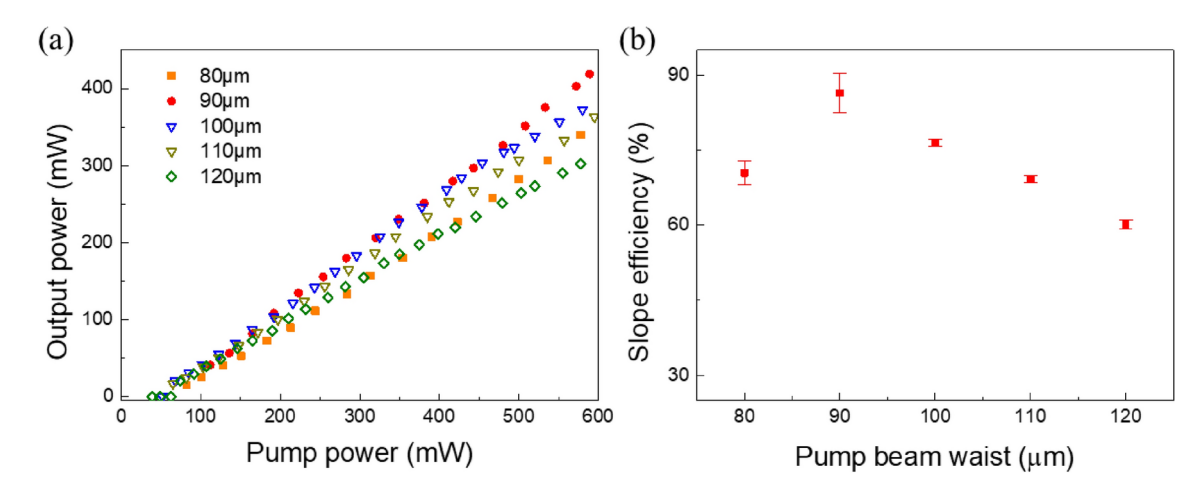


**Fig. 2.** (a) The output laser power versus the pump power for various pump beam waist diameters. (b) The slope efficiency as a function of the pump beam waist diameter. Here, the pump beam waist was located in the middle of the "Cs cell 2", whose temperature was maintained at 120 °C.

Pump beam waist diameter (μm)	80	90	100	110	120
Cavity length (mm)	133	136	140	143	145

Table 1. Cavity parameters for various pump beam waists.

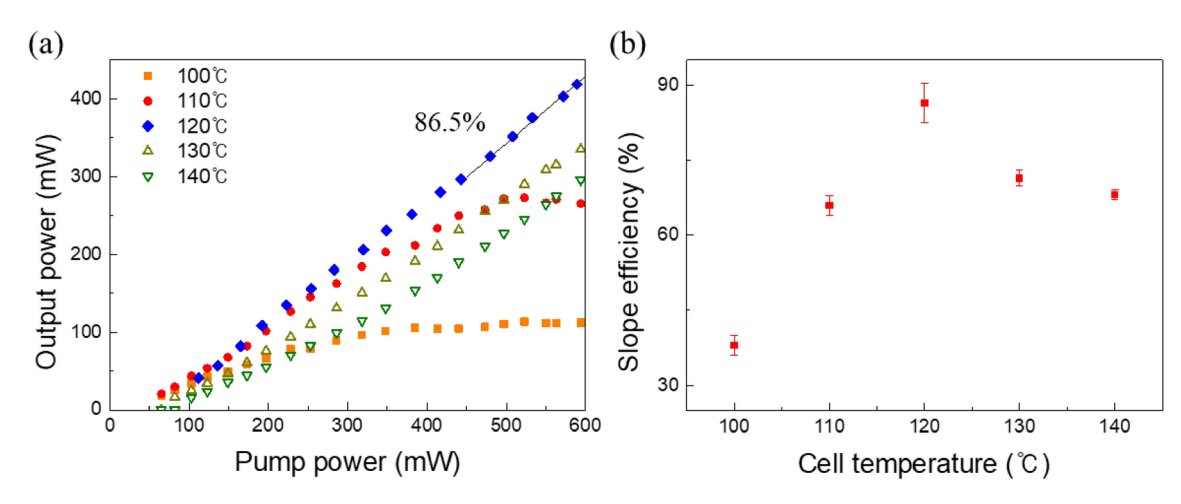


Fig. 3. (a) The output laser power versus the pump power for various Cs cell temperatures. (b) The slope efficiency as a function of the Cs cell temperature. Here, the pump beam waist was 90  $\mu$ m.

Note that the pump beam waist diameter was varied using the adjustable collimator, which also varied the cavity length as in Table 1 and, consequently, the laser cavity modes. Therefore, the laser output dependence on the pump beam waist diameter differs from the previous report<sup>47</sup>, where the cavity mode was fixed. A non-monotonic dependence of the slope efficiency on the pump beam waist in our experiments indicated that an optimal operation was within the range of the parameter variations in our experiments.

The cesium cell temperature determines the atomic density, partial pressure, and optical gain dynamics<sup>47,49</sup>. We experimentally optimized the temperature and measured its impact on laser output power, summarized in Fig. 3. In Fig. 3a, we observed saturation of laser power at the cell temperature of 100 and 110 °C such that the pump photon was not converted to laser photon proportionally. The saturation was not observed for the cell temperature over 120 °C, but the laser power and slope efficiency significantly varied. Figure 3b shows the slope efficiency as a function of cell temperature. The threshold power was measured to monotonically increase from ~15 mW at 100 °C to 162 mW at 140 °C. In contrast, the slope efficiency reached its maximum at the cell temperature of 120 °C and then decreased at higher temperatures. As temperature increases beyond the optimal point, more atoms are involved in mutual collisional processes, rapidly depopulating the excited state to result in a less population inversion and, subsequently, a lower optical gain.

Gain medium	OC R (%)	Slope efficiency (%)	O-to-O conversion (%)	Pump power (W)	Output power (W)	References
K	60	31	12	41.6	5	21
Cs	20	52	48	96	48	15
Rb	11	53	46	37	17	18
Cs	10	61.5	49	2.9	1.4	25
Cs	4	86.5	71	0.589	0.419	This work

Table 2. Comparison of laser characteristics of alkali atom lasers.(OC: output coupler, R: reflectivity).

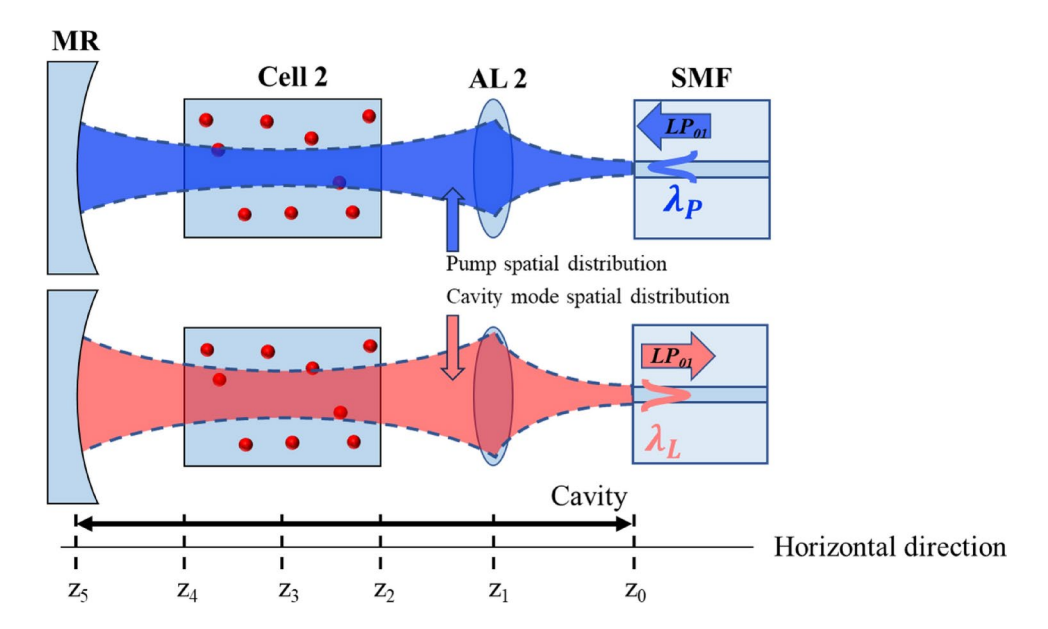


**Fig. 4.** Schematic diagram of the spatial distribution of the pump and the laser mode in the proposed hybrid cavity. The upper diagram illustrates the spatial distribution of the pump laser. The lower diagram shows the fundamental cavity mode configuration. At the bottom, the horizontal locations along the cell axis are marked  $(z_0)$ : fiber end facet,  $z_1$ : aspheric lens,  $z_2$ : the right window of Cell 2,  $z_3$ : the center of Cell 2,  $z_4$ : the left window of Cell 2,  $z_5$ : concave macroscopic reflector, MR: macroscopic reflector, AL: aspheric lens, SMF: single mode fiber).

	<b>z</b> <sub>5</sub>	<b>z</b> <sub>4</sub>	<b>z</b> <sub>3</sub>	<b>z</b> <sub>2</sub>	z <sub>1</sub>	z <sub>0</sub>
$w_p (\mu m)$	601	75.2	45	75.2	215.3	2.67
$w_L  (\mu m)$	607	77.3	46.8	76.2	216.9	2.78
Overlap	0.98	0.95	0.92	0.97	0.96	0.92

**Table 3.** Pump laser beam radius  $(w_P)$ , fundamental laser cavity mode radius  $(w_L)$ , and spatial overlap  $(w_P^2/w_L^2)$  at several axial positions.

For the optimal conditions with the pump waist of 90  $\mu m$  and the cell temperature of 120 °C, the proposed hybrid laser provided a slope efficiency of  $\sim$  86.5% and an optical-to-optical conversion efficiency of 71%, a substantial improvement over prior reports. Table 2 compares our results with some of the previous results.

The alkali atom vapor's high optical gain leads to a requirement of a low reflectivity of the OC<sup>48,50,51</sup> for optimal output power. Yet, the reflectivity in previous reports was still higher than 30%. Prior laser cavities adopted LD arrays with beam-forming optics to pump alkali atoms in a mixture of multiple high-order Gaussian beams. This inevitably incurred a spatial mismatch between the pump and the laser cavity modes. Our HC provided high slope efficiency by (1) securing a stably low reflectivity in the OC using the 4% Fresnel reflection at the interface between the glass fiber facet and air and (2) consistently increasing the spatial overlap between the pump and laser cavity mode.

In Fig. 4, we schematically showed how the spatial overlap was achieved in our proposed HC. Table 3 calculated the overlap between the pump beam and the fundamental cavity mode along the axial positions using ABCD matrix Gaussian beam optics<sup>52</sup>. The chromatic aberration of the aspheric lens due to the spectral separation between the pump ( $\lambda_P$  =852 nm) and laser ( $\lambda_L$ =894 nm) was considered. Still, the difference in the

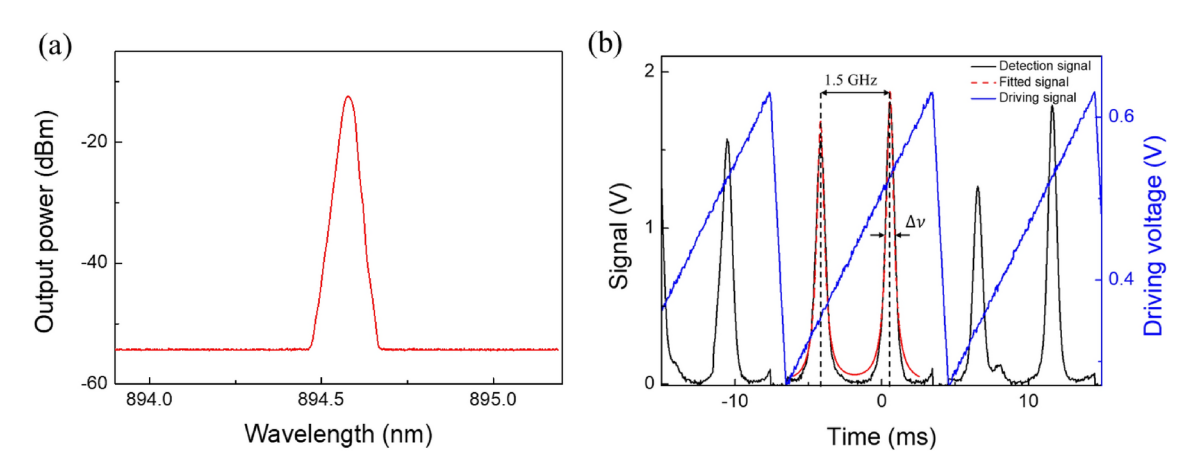


**Fig. 5**. Hybrid cavity output laser spectrum with (**a**) optical spectrum analyzer (OSA, Agilent 86142A) with 0.06 nm spectral resolution, and (**b**) scanning Fabry–Perot interferometer with a free spectral range (FSR) of 1.5 GHz and 60 finesse.

focal lengths between them was estimated to be  $\sim$  2  $\mu$ m, which was negligible in our experiments. It is noted that the spatial overlap was maintained over 0.92 within the cesium cell, which was not achievable in the prior cavities.

The slope efficiency of a laser is mainly determined by four factors as described in the equation below<sup>39</sup>:

$$\frac{dP_L}{dP_P} = \frac{\ln\left(1 - T\right)}{\ln\left(\left(1 - T\right)\left(1 - L\right)\right)} \frac{\lambda_P}{\lambda_L} \eta_P \frac{dS}{dF} \tag{1}$$

here, we have:  $dP_L/dP_P$ : slope efficiency,  $P_L$  laser power,  $P_P$ : pump power, T: transmission of the OC, L: total loss of cavity except for the transmission of the OC,  $\eta_P$ : ratio of the absorbed pump power over incident pump power, dS/dF: efficiency of converted laser photons from absorbed pump photons,  $\lambda_P$ : pump wavelength,  $\lambda_L$ : laser wavelength. T and L are in a range from 0 to 1. For the proposed HC,  $\lambda_P/\lambda_L=95.3\%$  T=96%, and we estimated L=6.7% (loss of aspheric lens = 0.2%, loss of concave mirror = 0.3%, cesium cell window loss = 6.2%) and notably  $\eta_P\sim$ 1. Compared to the previous report for Ti:Sapphire laser pumping  $^{39}$ , the term  $\frac{ln(1-T)}{ln((1-T)(1-L))}$  increased from 0.95 to 0.98, and dS/dF increased from 0.90 to 0.93 in our experiments. Matching the spatial overlap between the laser cavity mode and the pump, especially within the optical gain medium for  $z_2 < z < z_4$ , dS/dF increased meaning fully.

We measured the laser spectra in both wavelength and frequency domain. The results are summarized in Fig. 5. Using an optical spectrum analyzer (OSA, Agilent 86142A), we confirmed the lasing wavelength at 894.57 nm. See Fig. 5a. However, the OSA had a limited spectral resolution of 0.06 nm, and we further characterized the laser linewidth (Full-width Half-maximum),  $\Delta v$ , using a Fabry–Perot interfere meter (FPI, SA30-73) with 60 finesse. Using the FPI, the linewidth of the laser was measured to be 0.199 GHz, as in Fig. 5b.

The laser output was delivered in the  $LP_{01}$  mode of SMF, which served as an efficient spatial mode filter for the laser. We placed a beam profiler (Thorlabs, BP104-IR) at the position of the power meter in Fig. 1 and measured the beam quality of the laser output operating at the optimal condition. As expected, the  $M^2$  of the laser was highly symmetric and ranged from 1.04 to 1.08, comparable to those of low-power fiber lasers<sup>53</sup>.

Our study experimentally demonstrated the meaningful advantages of using SMF to form an HC by increasing the spatial overlap between the pump and laser mode within the gain medium. This method could find applications in laser systems where the pump and laser wavelengths are close in the spectral domain such that both could be guided in the  $LP_{01}$  mode of the optical fiber. Therefore, the proposed scheme can be applied to Raman and Brillouin laser with a macroscopic optical gain medium. Power scaling in the proposed HC might cause issues, such as optical damage at the optical fiber facet<sup>54</sup> and nonlinear optic effects in the fiber<sup>55–58</sup>. These hurdles might be alleviated using a large-mode-area fiber (LMAF) implemented in high-power laser delivery applications<sup>59,60</sup>, which the authors are pursuing.

# Conclusion

We proposed a new HC laser using cesium atom vapor as an optical gain medium. The cavity consisted of an MR with a high reflectivity of 99.7% and a fiber optic OC with ~4% Fresnel reflection. The single mode fiber also functioned as a passive mode-matching component to ensure a high overlap (>0.92) between the pump and laser cavity mode was maintained within the cesium optical gain cell. It also facilitated the low coupling losses for the laser to be guided in the  $LP_{01}$  mode of SMF. Optimizing the HC's physical parameters, such as the pump beam width of 90  $\mu$ m and the cell temperature of 120 °C, we achieved a slope efficiency of 86.5% and an optical-

to-optical conversion efficiency of 71%, which is significantly improved in comparison to prior reports. The laser output power was 419 mW at the pump power of 589 mW.

### Data availability

The datasets used and/or analysed during the current study are available from the corresponding author on reasonable request.

Received: 15 August 2024; Accepted: 13 February 2025

Published online: 03 March 2025

#### References

- 1. Bridges, W. B. Methods in Experimental Physics Vol. 15, 31-166 (Elsevier, 1979).
- 2. Kunii, T. & Matsui, Y. Narrow spectral linewidth semiconductor lasers. Opt. Quant. Electron. 24, 719-735 (1992).
- 3. Nasim, H. & Jamil, Y. Diode lasers: From laboratory to industry. Opt. Laser Technol. 56, 211-222 (2014).
- Geng, J., Wu, J., Jiang, S. & Yu, J. Efficient operation of diode-pumped single-frequency thulium-doped fiber lasers near 2 μm. Opt. Lett. 32, 355–357 (2007).
- 5. Nilsson, J. et al. High-power wavelength-tunable cladding-pumped rare-earth-doped silica fiber lasers. *Opt. Fiber Technol.* **10**, 5–30 (2004).
- 6. Mason, P. et al. Kilowatt average power 100 J-level diode pumped solid state laser. Optica 4, 438-439 (2017).
- 7. Fan, T. Y. & Byer, R. L. Diode laser-pumped solid-state lasers. IEEE J. Quant. Electron. 24, 895-912 (1988).
- 8. Han, J., Glebov, L., Venus, G. & Heaven, M. C. Demonstration of a diode-pumped metastable Ar laser. Opt. Lett. 38, 5458–5461 (2013).
- 9. Nilsson, J. & Payne, D. N. High-power fiber lasers. Science 332, 921-922 (2011).
- Richardson, D. J., Nilsson, J. & Clarkson, W. A. High power fiber lasers: Current status and future perspectives. JOSA B 27, B63–B92 (2010).
- 11. Cai, M., Painter, O., Vahala, K. & Sercel, P. Fiber-coupled microsphere laser. Opt. Lett. 25, 1430-1432 (2000).
- 12. Shayeganrad, G. Efficient design considerations for end-pumped solid-state-lasers. Opt. Laser Technol. 44, 987–994 (2012).
- 13. Wu, T. et al. Laser oscillation of Yb3+: Er3+ co-doped phosphosilicate microsphere. Appl. Opt. 53, 4747-4751 (2014).
- 14. Rashid, Z., Jonáš, A., Buczyński, R. & Kiraz, A. Optofluidic dye lasers based on holey fibers: Modeling and performance analysis. *J. Lightw. Technol.* 36, 4114–4122 (2018).
- 15. Vladev, V., Todorova, M., Brazkova, M. & Bozhkov, S. Diode-pumped all-fiber-optic liquid dye laser. Laser Phys. Lett. 18, 115103 (2021).
- 16. Nampoothiri, A. V. et al. Hollow-core optical fiber gas lasers (HOFGLAS): A review. Opt. Mater. Express 2, 948-961 (2012).
- 17. Zhou, Z. et al. Towards high-power mid-IR light source tunable from 38 to 45 μm by HBr-filled hollow-core silica fibres. *Light Sci. Appl.* 11, 15 (2022).
- 18. Stachowiak, D. in Photonics. 38 (MDPI).
- 19. Wrage, M. et al. Phase locking in a multicore fiber laser by means of a Talbot resonator. Opt. Lett. 25, 1436-1438 (2000).
- Cieslak, R. & Clarkson, W. Internal resonantly enhanced frequency doubling of continuous-wave fiber lasers. Opt. Lett. 36, 1896–
  1898 (2011).
- 21. Daniel, J. et al. Novel technique for mode selection in a multimode fiber laser. Opt. Express 19, 12434–12439 (2011).
- 22. Wu, Y. et al. High-energy, mid-IR, picosecond fiber-feedback optical parametric oscillator. Opt. Lett. 47, 3600–3603 (2022).
- 23. Zhdanov, B., Ehrenreich, T. & Knize, R. Narrowband external cavity laser diode array. *Electron. Lett.* 43, 1 (2007).
- 24. Zhdanov, B. V. & Knize, R. J. Review of alkali laser research and development. Opt. Eng. 52, 021010 (2012).
- 25. Gao, F. et al. Review on diode-pumped alkali vapor laser. Optik 124, 4353-4358 (2013).
- $26. \ \ Rabinowitz, P., Jacobs, S. \& Gould, G. Continuous optically pumped Cs laser. \textit{Appl. Opt. 1}, 513-516 (1962).$
- 27. Zhdanov, B., Sell, J. & Knize, R. Multiple laser diode array pumped Cs laser with 48W output power. Electron. Lett. 44, 1 (2008).
- 28. Zhdanov, B. V., Stooke, A., Boyadjian, G., Voci, A. & Knize, R. Rubidium vapor laser pumped by two laser diode arrays. *Opt. Lett.* 33, 414–415 (2008).
- 29. Endo, M., Nagaoka, R., Nagaoka, H., Nagai, T. & Wani, F. in Components and Packaging for Laser Systems IV. 83-92 (SPIE)
- Zhdanov, B., Shaffer, M., Sell, J. & Knize, R. Cesium vapor laser with transverse pumping by multiple laser diode arrays. Opt. Commun. 281, 5862–5863 (2008).
- 31. Zhdanov, B., Shaffer, M. & Knize, R. Cs laser with unstable cavity transversely pumped by multiple diode lasers. *Opt. Express* 17, 14767–14770 (2009).
- 32. Pitz, G. A. et al. in High Energy/Average Power Lasers and Intense Beam Applications IX. 9-16 (SPIE).
- 33. Zhdanov, B. V., Rotondaro, M. D., Shaffer, M. K. & Knize, R. J. Efficient potassium diode pumped alkali laser operating in pulsed mode. Opt. Express 22(14), 17266–17270 (2014).
- 34. Tan, Y., Xu, D., Li, Y., Jia, C., He, S., & Liu, W. 108 W diode pumped rubidium vapor laser with brewster angle structure. In 2021 IEEE 9th International Conference on Information, Communication and Networks (ICICN). (IEEE, 2021).
- 35. Hong, S., Kong, B., Lee, Y. S. & Oh, K. Optimization of diode-pumped cesium vapor laser using frequency locked pump laser. *Curr. Opt. Photon.* 2, 443–447 (2018).
- 36. Lee, M., Kim, S., Hong, S. & Oh, K. Hot alkali atomic vapor in laser technology development. New J. Phys. 26(10), 101201 (2024).
- 37. Pitz, G. A., Stalnaker, D. M., Guild, E. M., Oliker, B. Q., Moran, P. J., Townsend, S. W., & Hostutler, D. A. Advancements in flowing diode pumped alkali lasers. in *High Energy/Average Power Lasers and Intense Beam Applications IX*. Vol. 9729. SPIE, (2016).
- 38. Pitz, G. A. & Anderson, M. D. Recent advances in optically pumped alkali lasers. *Appl. Phys. Rev.* 4(4), 041101 (2017).
- 39. Zhdanov, B., Ehrenreich, T. & Knize, R. Highly efficient optically pumped cesium vapor laser. Opt. Commun. 260, 696-698 (2006).
- 40. Hwang, J., Jeong, T. & Moon, H. S. Hyperfine-state dependence of highly efficient amplification from diode-pumped cesium vapor. Opt. Express 27, 36231–36240 (2019).
- 41. Lee, M. et al. Bidirectional GHz bandwidth amplified spontaneous emission generation and high output power single-pass optical amplification through a hot Cs vapor cell. Opt. Contin. 1, 126–132 (2022).
- 42. Kim, H., Jeong, Y., Hwang, K., Yeom, D.-I. & Moon, H. S. Highly efficient diode-pumped alkali-vapor amplification with near-extreme-limit gain. *Opt. Express* 30, 25638–25646 (2022).
- 43. Marcuse, D. Loss analysis of single-mode fiber splices. Bell Syst. Tech. J. 56, 703-718 (1977).
- 44. Oh, K. & Paek, U.-C. Silica Optical Fiber Technology for Devices and Components: Design, Fabrication, and International Standards (Wiley, 2012).
- 45. Pitz, G. A., Fox, C. D. & Perram, G. P. Pressure broadening and shift of the cesium  $D_2$  transition by the noble gases and  $N_2$ ,  $H_2$ ,  $H_3$ ,  $H_4$ ,  $H_5$ ,  $H_5$ ,  $H_6$ ,  $H_6$ ,  $H_6$ ,  $H_7$ ,  $H_8$ ,  $H_9$ ,
- 46. Pitz, G. A., Fox, C. D. & Perram, G. P. Transfer between the cesium 6<sup>2</sup>P<sub>1/2</sub> and 6<sup>2</sup>P<sub>3/2</sub> levels induced by collisions with H<sub>2</sub>, HD, D<sub>2</sub>, CH<sub>4</sub>, C<sub>2</sub> H<sub>6</sub>, CF<sub>4</sub>, and C<sub>2</sub> F<sub>6</sub>. Phys. Rev. A **84**, 032708 (2011).

- 47. Cohen, T., Lebiush, E., Auslender, I., Barmashenko, B. D. & Rosenwaks, S. Influence of the pump-to-laser beam overlap on the performance of optically pumped cesium vapor laser. *Opt. Express* 24, 14374–14382 (2016).
- 48. Svelto, O. & Hanna, D. C. Principles of Lasers Vol. 4 (Springer, 1998).
- 49. Steck, D. A. Cesium D line data. (2003).
- 50. Wang, J. et al. Theoretical and experimental optimization of O-band multiwavelength mixed-cascaded phosphosilicate Raman fiber lasers. *IEEE Photon. J.* **3**, 633–643 (2011).
- 51. Krupke, W. F., Beach, R. J., Kanz, V. K., Payne, S. A. & Early, J. T. in High-Power Laser Ablation V. 7-17 (SPIE).
- 52. Kogelnik, H. & Li, T. Laser beams and resonators. Appl. Opt. 5, 1550-1567 (1966).
- 53. Pavlov, I., Ilbey, E., Dülgergil, E., Bayri, A. & Ilday, F. Ö. High-power high-repetition-rate single-mode Er-Yb-doped fiber laser system. Opt. Express 20, 9471–9475 (2012).
- 54. Carter, A. et al. in Laser-Induced Damage in Optical Materials: 2004. 561-571 (SPIE).
- 55. Aoki, Y. & Tajima, K. Stimulated Brillouin scattering in a long single-mode fiber excited with a multimode pump laser. *JOSA B* 5, 358–363 (1988).
- 56. Song, S., Jung, A. & Oh, K. High-temperature sensitivity in stimulated Brillouin scattering of 1060 nm single-mode fibers. *Sensors* 19, 4731 (2019).
- 57. Stolen, R. H., Lee, C. & Jain, R. K. Development of the stimulated Raman spectrum in single-mode silica fibers. *JOSA B* 1, 652–657 (1984)
- 58. Stolen, R. H. & Lin, C. Self-phase-modulation in silica optical fibers. Phys. Rev. A 17, 1448 (1978).
- 59. Li, L. et al. High power single transverse mode operation of a tapered large-mode-area fiber laser. Opt. Commun. 281, 655–657 (2008)
- 60. Thorlabs, [online] Available: http://www.thorlabs.com/.

### Acknowledgements

Not applicable.

#### **Author contributions**

S.K. contributed on the design of the work, acquisition, and was a major contributor in writing the manuscript. M.L. contributed on the design of the work. S.S. contributed on acquisition of data. S.H. contributed on the design of the work, and revised the draft. J.N. have substantially contributed on the substantially revised the draft. K.O. have substantially contributed on the interpretation of data, substantively revised the draft.

### **Funding**

This work was supported by the Institute for information & communications Technology Planning & Evaluation (IITP) grant funded by the Korea government (MIST) (No.2022-0-01029, Atomic ensemble-based quantum memory).

### **Declarations**

# Competing interests

The authors declare no competing interests.

#### Ethics approval

There is no ethics issue for this paper.

#### Consent for publication

All authors agreed to publish this paper.

# Additional information

Correspondence and requests for materials should be addressed to J.N. or K.O.

Reprints and permissions information is available at www.nature.com/reprints.

**Publisher's note** Springer Nature remains neutral with regard to jurisdictional claims in published maps and institutional affiliations.

**Open Access** This article is licensed under a Creative Commons Attribution-NonCommercial-NoDerivatives 4.0 International License, which permits any non-commercial use, sharing, distribution and reproduction in any medium or format, as long as you give appropriate credit to the original author(s) and the source, provide a link to the Creative Commons licence, and indicate if you modified the licensed material. You do not have permission under this licence to share adapted material derived from this article or parts of it. The images or other third party material in this article are included in the article's Creative Commons licence, unless indicated otherwise in a credit line to the material. If material is not included in the article's Creative Commons licence and your intended use is not permitted by statutory regulation or exceeds the permitted use, you will need to obtain permission directly from the copyright holder. To view a copy of this licence, visit <a href="http://creativecommons.org/licenses/by-nc-nd/4.0/">http://creativecommons.org/licenses/by-nc-nd/4.0/</a>.

© The Author(s) 2025